PHYSICAL REVIEW B VOLUME 61, NUMBER 6 1 FEBRUARY 2000-II

Compression mechanisms in the anisotropically bonded elements Se and Te

H. C. Hsueh, C. C. Lee, and C. W. Wang
Department of Physics, Tamkang University, Taiwan 25137, Republic of China

J. Crain
Department of Physics and Astronomy, The University of Edinburgh, Mayfield Road, Edinburgh EH9 3JZ, Scotland and IBM Research Division, 1623-14 Shimotsuruma, Yamato, 242-8502 Kanagawa, Japan

(Received 16 August 1999)

The compression mechanisms of the elements selenium and tellurium (which exhibit highly anisotropic bonding under ambient conditions) are explored. A combination of experiments and *ab initio* simulation (including generalized gradient corrections) is used to examine the structural and dynamic properties of these elements in detail. The effect of pressure on both these systems is to enhance the weak interchain bonding at the expense of the stronger intrachain covalent interactions. This is manifested by a pronounced mode softening of the intrachain vibrational modes under pressure as found from both Raman spectroscopy and simulation. A corresponding increase of the rigid-chain rotation mode is also revealed by the calculations. We also investigate pressure-induced polymorphism in these materials in order to resolve controversy concerning the high-pressure crystallographic structures.

I. INTRODUCTION

Observing the response of materials to hydrostatic compression is a powerful probe of complex bonding in solids. Of particular interest in this regard are anisotropic solids in which cohesive forces of very different strengths coexist. In recent years, major advances in experimental instrumentation for *in situ* high-pressure measurements and rapid increases in computer power have opened opportunities for detailed measurements of the structural and dynamical and electronic response to compression in complex materials.

The combination of x-ray diffraction, high-resolution optical spectroscopy, and *ab initio* simulation has revealed complex compression mechanisms in *layered* solids where electronic and vibrational properties show a clear cross over from quasi-two-dimensional to three-dimensional character under pressure while the crystallographic structure remains layered.[1,2] In certain families of molecular crystals, compression has been observed to induce intra- to inter-molecular electron transfer accompanied by a pronounced weakening of the intra-molecular bond strength and the formation of a two-dimensional layered solid.[3,4] Continued compression drives the layers closer together until a three-dimensional network solid of very low symmetry is formed. This process is accompanied by an unusual nonmonotonic variation of the intramolecular stretch frequency. In these cases *ab initio* simulation has been extremely effective in predicting and accounting for the complex compression mechanisms.

The group-VI elements Se and Te are, in principle, simpler than the compounds discussed above but are, nonetheless, known to be highly anisotropic under ambient conditions. These materials form chainlike structures with relatively strong covalent bonds in twofold coordination along the chain direction. Only weak cohesion exists between the chains. Despite their status as prototype anisotropic materials their compression mechanisms have not been explored at the same level of detail as for more complex materials. Attention has tended to focus on high-pressure metalization transitions to structures where the anisotropic chainlike bonding has been lost. Specifically, the equation of state has been measured using x-ray diffraction techniques[5–8] and detailed experimental structural studies have revealed a number of high-pressure phases of relatively low symmetry.[9,10] Theoretical calculations have been employed to examine the electronic structure of selenium and tellurium with a view to exploring successive pressure-driven transitions[11,12] and the appearance of superconductivity[13]. In the full-potential linearized-augmented-plane-wave method used by Geshi *et al.*[14] the calculated transition pressure is severely underestimated with respect to the experimental value. Still there have been several candidate high-pressure structures of Se and x-ray-diffraction methods have not yielded a definitive structure solution. There has also been some attention given to the liquid state semiconductor to metal transition.[15–17]

The compression mechanism of the ambient pressure phase of selenium and tellurium have not been explored in detail. Notable exceptions include recent Mössbauer studies[18] where the decrease of quadrupolar splitting with increasing pressure was attributed to the growing importance of interchain (interlayer) interactions in the trigonal phase.

The purpose of this paper is to draw together experimental results on Se and Te in order to understand the compression mechanism and to consider the accuracy with which simulation can account for the observations and to relate the structural and vibrational changes to electronic structure. We will also briefly consider high-pressure polymorphism in order to resolve existing controversy.

II. EXPERIMENTAL AND COMPUTATIONAL METHODS

A. Sample preparation and Raman scattering

Samples of Se and Te were obtained from Alfa Aesar products and used without further purification. The samples

were ground to a fine powder to minimize the effects of preferred orientation and loaded into a diamond anvil pressure cell without a pressure-transmitting medium.

High-pressure vibrational studies were carried out at the University of Edinburgh using Raman spectroscopy. Raman spectra were collected from a diamond anvil pressure cell in backscattering geometry using the 6764 Å line of a Kr^+ ion laser as the excitation source. The laser power was estimated to be 100 mW at the sample. The pressure was measured using ruby fluorescence. A Coderg T-800 triple-grating, scanning spectrometer was used for data collection. Spectral resolution was 1.5 cm^{-1} and count times were approximately 10 s.

B. Density-functional calculations

1. Electronic structure and equilibrium geometry

Density-functional[19] pseudopotential calculations were performed using an adaptation of the original CASTEP code[20] modified to perform full structural relaxation under the influence of arbitrary stresses and for symmetry-adapted normal-mode and frequency calculations. Here the equilibrium geometry was determined by relaxation under the influence of Hellmann-Feynman forces[21] and stresses using the methods described in Ref. 22. Nonlocal pseudopotentials were generated in the Kleinman-Bylander form using the Q_c tuning method.[23] The energy cutoff of 800 eV was used for the expansion of the plane-wave basis set. Structural relaxation proceeded until no force component exceeded 0.004 eV/Å where the calculated total energies were converged to better than 1 meV/atom. For calculations on the trigonal semiconducting phases, Brillouin-zone sampling is based on 14 special k points which correspond to the $5\times5\times4$ Monkhorst-Pack[24] k-point grid appropriate for the symmetry of the unit cell. Initial atomic positions were taken from experimental structural data at ambient pressure. Meanwhile, in an attempt to study the stability of high-pressure metallic phases of Se and Te, more k points for Brillouin-zone integration are necessary. We use an $8\times8\times3$ k-point grid and a $6\times4\times9$ k-point grid for the candidate high-pressure monoclinic structures with the space group of $C2/m$ and $P21$, respectively, which we find converges the total energy to 0.01 eV/atom. The Gaussian broadening technique with a broadening of 0.2 eV are performed to deal with the Fermi surface of the metallic structures.

2. Lattice dynamics calculations

For calculations of vibrational mode frequencies, a small set of displacements were made giving rise to harmonic restoring forces on all other atoms in the unit cell. Exploitation of space-group symmetry allowed for the construction of the full dynamical matrix which, when diagonalized, yields vibrational mode frequencies and associated eigenvectors. The details of phonon frequency calculations can be found elsewhere.[22,25] In this work we consider displacements in a single unit cell which therefore generate only Brillouin-zone center modes. We also compare our calculation with previous theoretical studies using frozen phonon calculation.

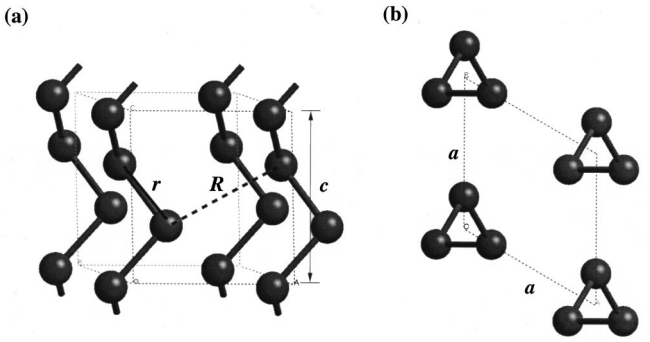

FIG. 1. Crystalline structure of ambient pressure structure of selenium and tellurium. Projection diagrams of the structure along the side view (a) and c axis (b) are shown, respectively. The intrachain and interchain distance denoted as r (solid line) and R (dashed line) are also shown.

III. RESULTS

A. Ambient pressure structures

The ambient pressure structures of selenium and tellurium are shown schematically in Fig. 1. The chainlike coordination of the atoms is evident. We define the nearest bonded neighbor distance (intrachain) as r and the nearest nonbonded (interchain) distance as R which can be determined from the structural parameters (a, c, and u) from the relations

$$r=\sqrt{3(ua)^2+\left(\frac{c}{3}\right)^2}, \tag{1}$$

$$R=\sqrt{a^2(1-3u)+r^2}. \tag{2}$$

These materials have $P3_121$ space-group symmetry. Group theory analysis predicts four zone center phonon modes of which three [two doubly degenerate (E' and E') and one nondegenerate (A_1)] are Raman active and one [nondegenerate (A_2)] mode is Raman silent. We find that local-density approximation (LDA) underestimates equilibrium volume (V_0) for both materials. The underestimate is primarily the result of overbound chains and the effect is more pronounced for Se. By contrast, generalized gradient approximation (GGA) calculations give V_0 in good agreement with experiment for Te but lead to an overestimate in the case of Se. The interchain separation for Se is again the origin of the discrepancy but in the GGA case the calculated interchain interaction is too weak. The intrachain bondlengths are reasonably well described for both materials using GGA calculations. The LDA calculations give intrachain bondlengths that are too long. The effect of the LDA is therefore to reduce the overall anisotropy of the cohesive forces as has been suggested in a previous calculation.[12] A summary of the structural results at ambient pressure is shown in Table I.

B. Structural response to compression

We first consider Te as the calculated ambient pressure structure is in good accord with experiment. The response to compression of the unit-cell dimensions are shown in Fig. 2(a) and the variation of the internal parameter u is shown in

TABLE I. Calculated and observed lattice constants (in Å), internal parameters (in fractional coordinate) intrachain distance r (in Å), interchain distance R (in Å), bond angle Θ (in deg), bulk modulus B_0 (in GPa), and the pressure derivative of bulk modulus B' for the trigonal selenium and tellurium at ambient pressure. GGA and LDA refer to the generalized gradient correction and local-density calculations, respectively. NCP and USP correspond to norm-conserving pseudopotentials and ultrasoft pseudopotentials, respectively.

	a	c	u	r	R	Θ	B_0	B'
				Se				
LDA(NCP) [a]	3.994	5.108	0.252	2.435	3.136	103.4	27.4	8.4
GGA(NCP) [a]	4.665	4.968	0.209	2.365	3.704	103.6	8.5	7.7
EXP [b]	4.368	4.958	0.225	2.375	3.438	103.3	14.9	2.3
EXP [c]	4.366	4.955	0.229	2.390	3.422	102.5		
LDA(NCP) [d]	4.12	5.06	0.243	2.42	3.43	103.2	16.8	
GGA(USP) [e]	4.413	5.119	0.226	2.43	3.49	103.8	7.1	
				Te				
LDA(NCP) [a]	4.270	5.913	0.285	2.886	3.312	101.6	35.3	8.1
GGA(NCP) [a]	4.521	5.866	0.269	2.821	3.510	102.8	14.6	10.1
EXP [b]	4.451	5.926	0.263	2.832	3.491	103.3	19.4	5.1
LDA(NCP) [f]	4.28	5.89	0.287	2.90	3.30	100.9	47.3*	7.0*
GGA(USP) [g]	4.571	5.988	0.269	2.919	3.543	101.0	18.0	

[a]Present work.
[b]Reference 26.
[c]Reference 28.
[d]Reference 29.
[e]Reference 16.
[f]Reference 30. * indicates at the reference pressure of 2 GPa.
[g]Reference 12.

Fig. 2(b). It is clear that the observed and calculated cell parameters are in good agreement. We extract the bulk modulus B_0 (shown in Table I) from fitting to the third-order Birch-Murnaghan equation of state. The values obtained from our GGA calculation are in good agreement with experimental results given in Ref. 26. By contrast, the sensitivity of the internal positional parameter to pressure is slightly overestimated in the GGA calculations. X-ray-diffraction measurements show a pronounced flattening of the pressure shift of the internal parameter whereas the calculation predicts a continued increase. A comparison of the observed and calculated value of R/r is shown in Fig. 3. We note that the experimental results indicate that this ratio approaches a constant value for both materials (about 1.3 and 1.2 for Se and Te, respectively) whereas the calculation suggests a continued decrease of the ratio. One might expect that compression should reduce the structural anisotropy in the material and that the ratio should approach unity under compression as

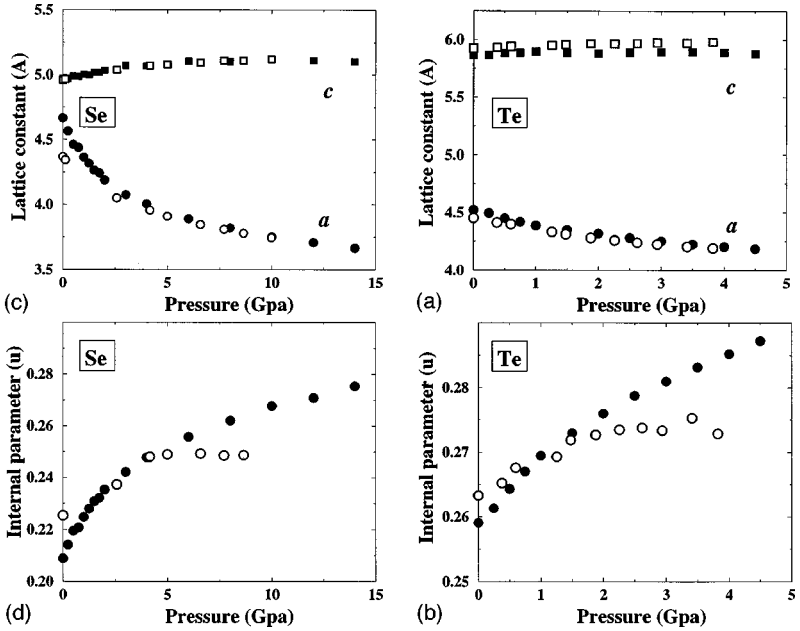

FIG. 2. The cell parameters (a and c) and internal structural parameter u of Te [(a) and (b)] and Se [(c) and (d)] as a function of pressure. Observed and calculated results are denoted as open and closed symbols, respectively.

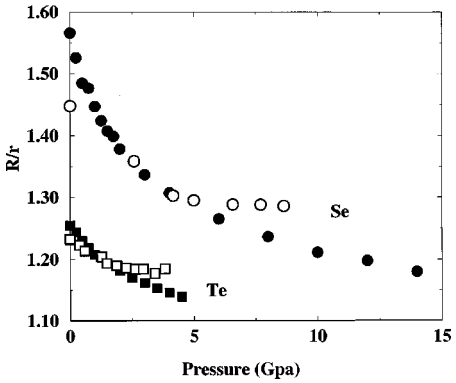

FIG. 3. The ratio of the R (interchain) and r (intrachain) as a function of pressure. The detail of calculating the bond distance can be found in the text. The open and closed symbols correspond, respectively, to the single-crystal x-ray-diffraction measurements and our calculations.

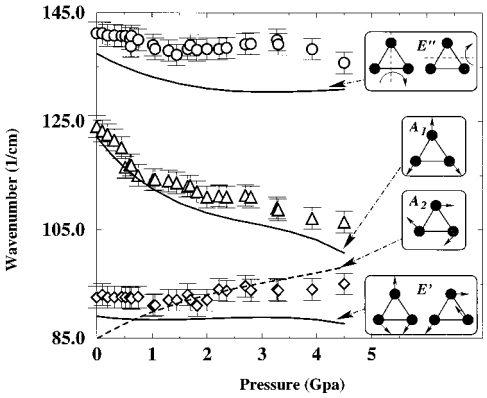

FIG. 4. The observed (open symbols with error bars) and calculated (solid curves) pressure shifts of the zone center Raman-active optical phonon frequencies of Te. Furthermore, the calculated Raman-silent A_2 frequency as a function of compression is shown as a dashed curve. The corresponding eigenvectors of specific phonon modes are also shown in schematic representations in which projection of the structure along the helix (c) axis is taken.

suggested in the calculations on both materials. It would be valuable to reexamine the high-pressure structural response of these two materials using image plate area detectors to confirm the detailed behavior of the internal compression mechanism. We also note that our calculation corresponds to 0 K and that thermal effects are not included though they may play a role in the high-pressure response. High-pressure diffraction measurements at low temperature would therefore be of particular value.

C. Vibrational behavior under pressure

The ambient pressure vibrational frequencies for Se and Te are shown in Table II and our calculated GGA values compare well with experiment and a previous GGA frozen phonon calculation.[16] We note that a previous LDA calculation[16] seriously overestimates the frequency of the A_2 mode and underestimates that of the A_1 mode. We now consider the high-pressure response of the vibrational frequencies and consider Te first.

TABLE II. Observed and calculated frequencies (in units of cm^{-1}) of the zone-center optic modes in trigonal Se and Te under ambient pressure. R_a and R_s denotes the Raman-active and Raman-silent mode, respectively.

	$E''(R_a)$	$A_1(R_a)$	$E'(R_a)$	$A_2(R_s)$
		Se		
GGA(NCP) [a]	242.9	223.5	144.5	108.6
EXP [b]	231	237	142	102
EXP [c]	235.5	238.6	148.7	
LDA(USP) [d]		177.8		136.0
GGA(USP) [d]		217.6		94.5
		Te		
GGA(NCP) [a]	138.7	120.2	86.8	82.4
EXP [a]	141.2	124	92.5	
EXP [b]	142	122	93	88
EXP [c]	141.5	121.4	92.3	

[a]Present work.
[b]Reference 31.
[c]Reference 32.
[d]Reference 16. Frozen-phonon calculations.

The response to compression of the zone-center optical phonons is shown in Fig. 4. We consider first the A_1 mode which corresponds to the symmetric intrachain dilation and compression mode normal to the chain axis. Since the chain is a helical structure, this mode involves *both* bond-length and bond-angle distortions. Here, significant mode softening with pressure is observed and quantitative agreement between experiment and calculation across the entire pressure range of the experimental measurements is found. We also consider the A_2 mode which corresponds to pure rigid-chain rotation and which is silent in Raman scattering. Its pressure response is therefore only accessible to us through the calculations. We find that this mode frequency increases significantly under compression and becomes comparable to the frequency of the intrachain dilation mode (A_1) at pressures of 4.5 GPa. Clearly this suggests an increase of interchain interaction at the expense of intrachain bonding. We also

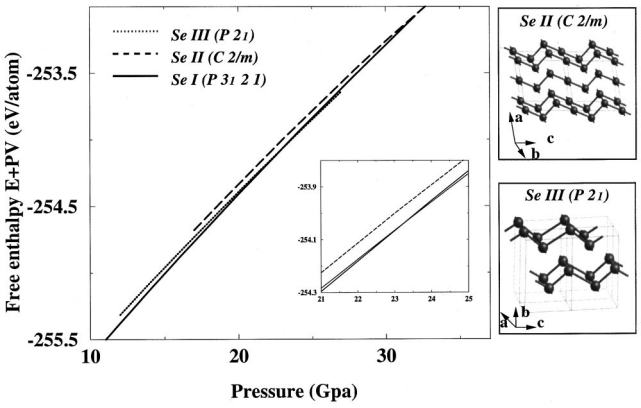

FIG. 5. The free enthalpy per atom as a function of atomic volume for the trigonal SeI($P3_121$) and monoclinic SeII($C2/m$) and SeIII($P2_1$) phases is shown as the solid, dotted, and dashed line, respectively. Schematic models for two monoclinic structures are also shown in the inset.

consider two other modes: These are intrachain modes corresponding to axial helix compression and asymmetric dilation (normal to the helix axis). At ambient pressure, the displacement eigenvectors corresponding to these two modes show significant admixture. Under compression, the two modes decouple giving two pairs of degenerate displacement patterns with assigned to E'' and E' symmetry (see Fig. 4). Similar results are found for Se.

D. High-pressure phases

In this section we examine candidate high-pressure polymorphs of Se and Te. Our aim is to explore the structural transformations accompanying the semiconductor to metal transition. We consider two competing candidate structures that have been proposed for selenium.[9,17] The structures are shown in the inset to Fig. 5. Due to the similarity of the structures, x-ray-diffraction methods have not led to a decisive structure solution for the lowest pressure metallic phase. In particular we consider two monoclinic layered structures (space groups $C2/m$ and $P2_1$). The stacking sequence for both structures is identical (*ABAB*), however, the $C2/m$ structure includes 180° bond angles which are absent from the $P2_1$ structure. From our total-energy calculations we find that the $C2/m$ phase is the stable high-pressure metallic structure (detailed electronic structure analysis of the $C2/m$ phase of Se can be found in Ref. 33). Specifically we identify a phase-transition pressure of roughly 23 GPa at which point the difference in enthalpy between the candidate structures is about 0.05 eV/atom (see Fig. 5 and Table III). Although this is a small difference it is, nonetheless, above the numerical uncertainty in our calculation. We further note that the $P2_1$ structure is never stable relative to the $C2/m$ over the full pressure range considered. Our calculated transition pressure is, however, significantly higher than the experimental metallization pressure of 14GPa.[9] One possible explanation for the discrepancy is the fact that our calculation corresponds to 0 K whereas existing high-pressure diffraction measurements have all been performed at room temperature. There is evidence to suggest that the metallization phase transition in Te shifts to higher pressures upon cooling[27] and the same effect may be present in Se.

IV. CONCLUSION

In conclusion we have examined in detail the compression mechanisms of quasi-one-dimensional elements Se and Te under hydrostatic pressure. Changes in structural and dynamical properties suggest that the intrachain bonds weaken under pressure as interchain interactions become stronger thereby reducing the overall anisotropy. This is accompanied by a significant increase in the interchain rotational mode frequency and is well accounted for by density-functional theory including gradient corrections. Energy considerations also suggest that the ambient trigonal phase becomes unstable with respect to a low-symmetry layered metallic phase at pressures above 23 GPa for Se. We suggest that low-temperature x-ray-diffraction measurements would be useful to confirm our predictions.

TABLE III. Calculated structural parameters (a, b, and c in units of Å , and β in deg) and atomic volume V (in Å ^{3}) at various pressure P (in GPa) with corresponding space groups are shown. The calculated $E+PV$ (in eV) gives the structural free enthalpy difference per atom relative to the trigonal structure at ambient pressure. The corresponding experimental data are also shown in parentheses.

P	Space group	a	b	c	β	V	$E+PV$
				Se			
17	$C2/m$ [a]	6.721	2.696	6.278	105.55	18.27	5.65
	[b]	(6.57)	(2.69)	(6.29)	(105.4)	(17.86)	
	$P2_1$ [a]	4.415	6.462	2.594	89.92	18.50	5.70
23	$C/2m$ [a]	6.477	2.651	6.284	105.24	17.35	6.32
	$P2_1$ [a]	4.203	6.264	2.645	90.27	17.41	6.38
	[c]	(4.601)	(6.448)	(2.658)	(93.33)	(17.35)	

[a]Present work.
[b]Reference 17.
[c]Reference 19.

ACKNOWLEDGMENTS

We thank H. Vass for his help in maintaining and preparing the Raman-scattering facilities. We also wish to thank M. H. Lee and G. J. Ackland for useful discussions. This work was supported by a grant from National Science Council, Taiwan, R.O.C., Grant No. NSC-89-2112-M-032-013. J.C. thanks the Royal Society for support.

[1] H. C. Hsueh, H. Vass, S. J. Clark, G. J. Ackland, and J. Crain, Phys. Rev. B **51**, 16 750 (1995).
[2] H. C. Hsueh, M. C. Warren, H. Vass, G. J. Ackland, S. J. Clark, and J. Crain, Phys. Rev. B **53**, 14 806 (1996).
[3] H. C. Hsueh, Roger K. Chen, H. Vass, S. J. Clark, G. J. Ackland, W.C-K. Poon, and J. Crain, Phys. Rev. B **58**, 14 812 (1998).
[4] H. C. Hsueh and J. Crain, Phys. Status Solidi B **211**, 365 (1999).
[5] G. Parthasarathy and W. Holzapfel, Phys. Rev. B **37**, 8499 (1988).
[6] G. Parthasarathy and W. Holzapfel, Phys. Rev. B **38**, 10 105 (1988).
[7] T. Krüger and W. Holzapfel, Phys. Rev. Lett. **69**, 305 (1992).
[8] W. Holzapfel, Rep. Prog. Phys. **59**, 29 (1996).
[9] Y. Akahama, M. Kobayashi, and H. Kawamura, Phys. Rev. B **47**, 20 (1993).
[10] K. Aoki, O. Shimomura, and S. Minomura, J. Phys. Soc. Jpn. **48**, 551 (1980).
[11] D. Singh, A. K. Bandyopadhyay, M. Rajagopalan, P. Ch. Sahu, M. Yousuf, and K. Govinda Rajan, Solid State Commun. **109**, 339 (1999).
[12] G. Kresse, J. Furthmüller, and J. Hafner, Phys. Rev. B **50**, 13 181 (1994).
[13] F. Mauri, O. Zakharov, S. de Gironcoli, S. G. Louie, and M. L. Cohen, Phys. Rev. Lett. **77**, 1151 (1996).

[14] M. Geshi, T. Oda, and Y. Hiwatari, J. Phys. Soc. Jpn. **9**, 3141 (1998).
[15] Y. Soldo, J. L. Hazemann, D. Aberd, M. Inui, K. Tamura, D. Raoux, E. Pernot, D. F. Jal, and J. Dupuy Philon, Phys. Rev. B **57**, 258 (1998).
[16] F. Kirchhoff, G. Kresse, and M. J. Gillan, Phys. Rev. B **57**, 10 482 (1998).
[17] Y. Ohmasa, I. Yamamoto, M. Yao, and H. Endo, J. Phys. Soc. Jpn. **64**, 4766 (1995).
[18] P. Vulliet and J. Sanchez, Phys. Rev. B **58**, 171 (1998).
[19] W. Kohn and L. J. Sham, Phys. Rev. **140**, A1133 (1965).
[20] M. C. Payne, M. P. Teter, D. C. Allan, T. A. Arias, and J. D. Joannopoulos, Rev. Mod. Phys. **64**, 1045 (1992).
[21] R. P. Feynman, Phys. Rev. **56**, 340 (1939).
[22] H. C. Hsueh, H. Vass, S. J. Clark, and J. Crain, Europhys. Lett. **31**, 151 (1995).
[23] J. S. Lin, A. Qteish, M. C. Payne, and V. Heine, Phys. Rev. B **47**, 4174 (1993).
[24] H. J. Monkhorst and J. D. Pack, Phys. Rev. B **13**, 5188 (1976).
[25] H. C. Hsueh, F. N. Pu, S. J. Clark, H. Vass, and J. Crain, Europhys. Lett. **38**, 107 (1997).
[26] R. Keller, W. B. Holzapfel, and H. Schulz, Phys. Rev. B **16**, 4044 (1977).
[27] V. V. Brazhkin, R. N. Voloshin, S. V. Popova, and A. G. Umnov, J. Phys.: Condens. Matter **4**, 1419 (1992).
[28] D. Vanderbilt and J. D. Joannopoulos, Phys. Rev. B **27**, 6296 (1983).
[29] H. Akbarzadeh, S. J. Clark, and G. J. Ackland, J. Phys.: Condens. Matter **5**, 8065 (1993).
[30] F. Kirchhoff, N. Binggeli, G. Galli, and S. Massidda, Phys. Rev. B **50**, 9063 (1994).
[31] G. Lucovsky, Phys. Status Solidi B **49**, 633 (1972).
[32] W. Richter, J. B. Renucci, and M. Cardona, Phys. Status Solidi B **56**, 223 (1973).
[33] M. Geshi, T. Oda, and Y. Hiwatari, J. Phys. Soc. Jpn. **68**, 3341 (1999).